4 VARIABLES AFFECTING INSTRUMENT MINIMUM DETECTABLE CONCENTRATIONS

Before the MDC for a particular instrument and survey procedure can be determined, it is necessary to introduce the expression for total alpha or beta surface activity per unit area. The International Standard ISO 7503-1, "Evaluation of Surface Contamination," recommends that the total surface activity, A_s, be calculated similarly to the following expression:

$$A_s = \frac{R_{S+B} - R_B}{(\epsilon_i)(W)(\epsilon_s)} \tag{4-1}$$

where,

R_{S+B} = the gross count rate of the measurement in cpm,
R_B = the background count rate in cpm,
ϵ_i = the instrument or detector efficiency (unitless),
ϵ_s = the efficiency of the contamination source (unitless), and
W = the area of the detector window (cm^2).

(For instances in which W does not equal 100 cm^2, probe area corrections are necessary to convert the detector response to units of dpm per 100 cm^2.)

This expression clearly distinguishes between instrument (detector) efficiency and source efficiency. The product of the instrument and source efficiency yields the total efficiency ϵ_{tot}. Currently, surface contamination is assessed by converting the instrument response to surface activity using one overall total efficiency. This is not a problem provided that the calibration source exhibits characteristics similar to the surface contamination—including radiation energy, backscatter effects, source geometry, self-absorption, etc. In practice this is hardly the case; more likely, total efficiencies are determined with a clean, stainless steel source, and then those efficiencies are used to measure contamination on a dust-covered concrete surface. By separating the efficiency into two components, the surveyor has a greater ability to consider the actual characteristics of the surface contamination.

The instrument efficiency is defined as the ratio between the net count rate of the instrument and the surface emission rate of a source for a specified geometry. The surface emission rate, $q_{2\pi}$, is defined as the "number of particles of a given type above a given energy emerging from the front face of the source per unit time" (ISO 7503-1). The surface emission rate is the 2π particle fluence that embodies both the absorption and scattering processes that affect the radiation emitted from the source. Thus, the instrument efficiency is determined by

$$\epsilon_i = \frac{R_{S+B} - R_B}{q_{2\pi}} \tag{4-2}$$

The instrument efficiency is determined during calibration by obtaining a static count with the detector over a calibration source that has a traceable activity or surface emission rate or both. In many cases, it is the source surface emission rate that is measured by the manufacturer and certified as National Institute of Standards and Technology (NIST) traceable. The source activity

is then calculated from the surface emission rate based on assumed backscatter and self-absorption properties of the source. The theoretical maximum value of instrument efficiency is 1.

The source efficiency, ϵ_s, is defined as the ratio between the number of particles of a given type emerging from the front face of a source and the number of particles of the same type created or released within the source per unit time (ISO 7503-1). The source (or surface) efficiency takes into account the increased particle emission due to backscatter effects, as well as the decreased particle emission due to self-absorption losses. For an ideal source (no backscatter or self-absorption), the value of ϵ_s is 0.5. Many real sources will exhibit values of ϵ_s less than 0.5, although values greater than 0.5 are possible, depending on the relative importance of the absorption and backscatter processes. Source efficiencies may either be determined experimentally or simply selected from the guidance contained in ISO 7503-1 (refer to Section 5.3.2).

This current section considers some of the factors that affect the instrument efficiency ϵ_i. These detector-related factors include detector size (probe surface area), window density thickness, geotropism, instrument response time, and ambient conditions such as temperature, pressure, and humidity. The instrument efficiency also depends on the radionuclide source used for calibration and the solid angle effects, which include source-to-detector distance and source geometry.

Section 5 covers some of the factors that affect the source efficiency ϵ_s. Among these source-related factors are the type of radiation and its energy, source uniformity, surface roughness and coverings, and surface composition (e.g., wood, metal, concrete).

4.1 Radionuclide Sources for Calibration

For accurate measurements of total surface activity, it is essential that field instruments be calibrated appropriately. The MDC of an instrument depends on a variety of parameters, one of which involves the selection of calibration sources. Calibration sources should be selected that emit alpha or beta radiation with energies similar to those expected of the contaminant in the field. ISO-8769, "Reference Sources for the Calibration of Surface Contamination Monitors," provides recommendations on calibration source characteristics. As discussed in Section 5.5, the most representative calibration source would be one prepared from the radioactive material being assessed in the field. For example, both the uranium and thorium series emit a complex decay scheme of alpha, beta and gamma radiations—calibration to a single radionuclide must carefully be assessed to ensure that it is representative of the detector's response to these decay series.

An instrument's MDC depends on the type and energy of radiation. The radionuclides selected for this study were chosen so that they represent the types or the range, or both, of energies commonly encountered in decommissioned facilities. These radionuclides are C-14, Ni-63, SrY-90, Tc-99, and Tl-204 for beta measurements, and Th-230 and Pu-239 for alpha measurements. The calibration sources, available at ESSAP facilities, are traceable to NIST standards. Generally, the sources are of three geometric shapes: "button" sources (simulating a point source, approximately 5 cm^2), disc sources that cover a standard area of approximately 15 cm^2, or distributed sources that typically range from 126 to 150 cm^2. Table 4.1 summarizes the calibration sources used in this study.

The efficiencies determined in this section are for ideal laboratory conditions, which include the use of smooth, clean calibration source surfaces. Table 4.2 presents the average total efficiencies for the gas proportional, GM, and ZnS detectors compiled from historical calibration data at ESSAP. Table 4.3 provides MDCs that were calculated for the gas proportional detector ($\alpha + \beta$ mode) and the GM detector using the ambient background count rates provided in Table 5.1 and the total efficiencies in Table 4.2. As expected, the MDCs decrease with increasing beta energy. This is shown graphically in Figures 4.1 and 4.2 for the gas proportional and GM detectors, respectively. For beta energies (beta endpoint energies are used here) ranging from 300 to 1400 keV, the calculated MDCs are generally constant. However, the MDCs increase rapidly with decreasing beta energies below 300 keV.

The determination of source efficiencies in Section 5 required the assessment of instrument efficiencies under specific experimental conditions. These conditions included active area of source, detector specifications, and a source-to-detector geometry that included two sheets of Mylar. Table 4.4 shows results of instrument efficiencies determined under these conditions.

4.2 Source-to-Detector Distance

The distance between a source and the detector is another factor that may affect the instrument efficiency and, thus, the MDC. In this study, instrument MDC was evaluated as a function of distance from the source. The range of distances was selected to be appropriate for the type of radiation being measured, and in consideration of the typical detector-to-surface distances encountered in the course of performing surveys in support of decommissioning. Counts of 1 minute in duration were made with the detector at various distances above the source.

The source-to-detector distance was evaluated using a Ludlum Model 43-68 gas proportional detector with a 0.8 mg/cm^2 window for beta emitters, including C-14, Ni-63, SrY-90, Tc-99 (two source geometries were used), and Tl-204, and for Pu-239 and Th-230 (two source geometries were used). Five 1-minute measurements were made at contact and at distances of 0.5 cm, 1 cm, and 2 cm. The distances were obtained by cutting out the specified thicknesses of plastic and using them to maintain the desired source-to-detector spacing. Tables 4.5 and 4.6 show the results of an increasing source-to-detector distance on instrument response. Specifically, the net count rate obtained at each distance was normalized to the net count rate obtained in contact with the source. These results demonstrate the significant reduction in instrument response that can occur when source-to-detector distance is increased by less than 1 cm.

As was expected, the greatest reduction in detector response per increased distance from the source was obtained for the alpha and low-energy beta emitters, i.e., Ni-63 and C-14. The modest reduction in instrument response for the alpha-emitting Pu-239 and Th-230 sources, from being in contact with the source to 1 cm, was somewhat unexpected. The C-14 and Ni-63 exhibited equal or greater reductions in instrument response over this range compared to the alpha emitters. Somewhat more anticipated was the dramatic reduction in instrument response from 1 to 2 cm for the Pu-239 and Th-230 sources. The instrument response to the Th-230 disc source

at 2 cm was only 4% of the response obtained in contact with the source. This was contrasted to the Pu-239 disc source that exhibited 20% of the response at 2 cm relative to the contact measurement. The greater instrument response of Pu-239 at 2 cm relative to Th-230 at the same distance was likely due to the higher energy of the Pu-239 alpha emission (i.e., 5.1 MeV for Pu-239 versus 4.7 MeV for Th-230).

The data presented in Tables 4.5 and 4.6 were used to determine total efficiencies as a function of detector-to-source distance. It should be noted that although total efficiencies were determined and reported at each distance, the detector-to-source distance influences the instrument efficiency ϵ_i (as opposed to ϵ_s). These total efficiencies were used to calculate the MDCs presented in Tables 4.7 and 4.8. Figures 4.3 and 4.4 illustrate the effects of source-to-detector distance on the MDC for the beta emitters. These figures show that the source-to-detector distance effect on MDCs was relatively minor for the higher energy beta emitters (e.g., SrY-90 and Tl-204), but considerable for the low to mid-energy beta emitters. Figure 4.5 shows the effects of source-to-detector distance on the MDC for alpha emitters. For alpha emitters, the MDCs gradually increased as the detector-to-source spacing increased from contact to 1 cm. At 2-cm distance, consistent with the substantial reduction in total efficiency, the MDCs increased significantly. The MDC determined for Ni-63 at a detector-to-source distance of 2 cm was 52,000 ± 56,000 dpm/100 cm^2, with the relatively large uncertainty attributed to the error in the total efficiency determination. This magnitude of uncertainty in the MDC term suggests that the detection capability for the measurement process, i.e. detecting Ni-63 with a gas proportional detector 2 cm from the surface, is likely overestimated. This particular example illustrates the need for adjusting the MDC to account for uncertainties in the calibration factors (refer to Section 3.1 for discussion of MDC adjustment factor).

The practicality of these results may be realized by the deviation in instrument response that results when the source-to-detector distance during calibration is only slightly different (i.e., less than 1 cm for some radionuclides) from the detector-to-surface spacing maintained during field measurements of surface activity. That is, small changes in detector-to-surface distance produce significant changes in detector response, especially for alpha and low-energy beta radiation (1 to 2 cm spacing is not unusual for a roughly scabbled concrete surface). The effects on Tl-204 and SrY-90, although less than those on lower energy beta emitters, were still appreciable.

To minimize the effects of source-to-detector distance on MDCs, it is recommended that the detector be calibrated at a source-to-detector distance that is similar to the expected detector-to-surface spacing in the field.

4.3 Window Density Thickness

The detector-related factors that may change the instrument MDC are detector size (probe surface area), window density thickness, geotropism, instrument response time, and ambient conditions such as temperature, pressure, and humidity. In many instances, this information is already available. For example, the effects of ambient conditions and geotropism are usually tested by users concerned about the instrument or detector performance (Swinth & Kenoyer 1984; LA-10729).

One detector-related factor evaluated in this report was the effect of window density thickness on instrument response (using the Ludlum model 43-68) for C-14, Ni-63, Sr-90, Tc-99 (two source geometries were used for Tc-99), and Tl-204. Window density thickness for gas proportional detectors may be varied to provide a mechanism to control instrument response to various surface activity conditions. For example, in the assessment of low-energy beta emitters, a relatively thin window (e.g., 0.4 mg/cm^2) provides greater sensitivity. Similarly, when beta radiation in the presence of alpha radiation must be assessed, it is possible to selectively discriminate out the alpha radiation using an alpha shield (i.e., using 3.8 mg/cm^2 window density thickness).

Measurements were performed for window density thicknesses of 0.3, 0.4, 0.8, and 3.8 mg/cm^2. In addition, MDC measurements at window density thicknesses of 1.3, 1.8, 2.3, 2.8, and 3.3 mg/cm^2 were performed for the two Tc-99 source geometries. Window density thicknesses were varied by adding sheets of 0.5-mg/cm^2 Mylar between the source and the detector. The results of these measurements are given in Table 4.9. Figures 4.6 and 4.7 illustrate the effects of window density thickness on the total efficiency. The total efficiency was reduced more significantly for the lower energy beta emitters as the window density thickness was increased.

The total efficiencies presented in Table 4.9 were used to determine MDCs as a function of window density thickness (Table 4.10). Figures 4.8 and 4.9 illustrate the effects of window density thickness on the MDC for the beta emitters. These figures show, as did the source-to-detector distance evaluation, that the window density thickness over the range of 0.3 to 3.8 mg/cm^2 has a trivial effect on MDCs for the higher energy beta emitters (e.g., SrY-90 and Tl-204), but was considerable for the low to mid-energy beta emitters. These figures illustrate how the detector MDC calibrated to lower energy beta emitters is significantly affected by the window density thickness. As with the effects of source-to-detector distance on MDCs, it is essential that the detector be calibrated with the same window density thickness that will be used for survey measurements in the field. This concern may arise if the window is replaced in the field with one of a different thickness and returned to service without recalibration.

4.4 Source Geometry Factors

The source geometry must be considered in determining the instrument MDC. The detector's response may be influenced, in part, by the contaminant's distribution on the surface being assessed. For example, if the contamination can be characterized by relatively large uniform areas of activity, then the detector should be calibrated to a distributed or extended source. Similarly, if the surface can be characterized by localized spots of surface contamination, that may be approximated by a point source, then the calibration source should be similar to a point source geometry.

The source geometry effect on detector response was evaluated by determining the instrument efficiencies (ϵ_i) for gas proportional, GM, and ZnS detectors placed in contact with both distributed and disc sources. The radionuclide sources used in this evaluation were Tc-99 and Th-230. The instrument efficiencies determined for each detector and geometry configuration are shown in Table 4.11. The instrument efficiencies determined with the disc sources were 6 to 42% greater than those obtained with the distributed sources. These results were expected because of the solid angle of the measurement geometry. That is, for the smaller disc source, a larger

fraction of the radiation particles (α and β) emitted from the source intersect the detector probe area. Walker (1994) provides further information on the effects of source-to-detector geometry.

During the course of performing field survey measurements, it would be a time-consuming task to determine the contaminant geometry at each measurement location in an effort to select the most appropriate instrument efficiency. The benefits of a better defined contaminant geometry should be weighed against the increased labor expended in characterizing the contamination. It may be appropriate (conservative) to use the instrument efficiency obtained from a distributed source geometry for all surface activity measurement locations, except for those locations of elevated direct radiation. Only for locations of elevated direct radiation would effort be warranted to characterize the contaminant geometry in order to select the most appropriate instrument efficiency. Additionally, ISO-8769 recommends that the calibration source dimensions be sufficient to provide an area of 150 cm^2—certainly a distributed source.

4.5 Ambient Background Count Rate

The effects of ambient background (in particular, relatively high ambient background) on the calculated MDC and measured activity concentration of a radioactive source using a GM detector were evaluated. The procedure included collecting five 1-minute measurements of the ambient background, followed by five 1-minute measurements of a NIST-traceable Tc-99 disc source (activity concentration was 1,500 dpm within a 5-cm^2 active area). A jig was used to ensure that a reproducible geometry was maintained for each measurement. The ambient background was increased by placing Cs-137 sources at various distances from the GM detector. The ambient background levels ranged from approximately 50 to 1,500 cpm. This procedure allowed a comparison of the *a priori* MDC and the measured activity concentration of the Tc-99 source. The measured activity concentration was calculated using a total efficiency of 0.17 count per disintegration (from Table 4.2); no probe area correction was made since it was known that the source activity was limited to a 5-cm^2 area. Results are tabulated in Table 4.12.

As expected from the MDC equation, the calculated detection sensitivity (or MDC) of the GM detector increased directly with the square root of the ambient background level (Figure 4.10). For ambient background levels ranging from 50 to 145 cpm (consistent with background levels typically encountered during final status surveys), the measured activity of the Tc-99 was very similar to the stated activity of the source. As the ambient background levels were increased to 1,000 cpm, the measured activity was, with one exception, consistently lower than the certified source activity. As the ambient background was further increased to 1,500 cpm, the measured activity was less than 60% of the certified source activity, with significant uncertainty at the 95% confidence level.

In general, as the ambient background increases, and the ratio of the calculated MDC to the actual activity concentration present approaches unity, the uncertainty in the measured activity increases. However, only when the calculated MDC was approximately 70% of the actual activity concentration (MDC equal to 1,070 dpm per 5 cm^2), was there significant uncertainty and inaccuracy in the measured activity. For the case in which the MDC is a small fraction of the guideline value, significant uncertainty in the value is acceptable (e.g., ±100% uncertainty in a value that is 20% of the guideline gives adequate assurance that the compliance with the guideline has been achieved). If this is not the case, caution must be exercised when making measurements

that are close to the MDC, because substantial uncertainties may be associated with the measurements.

Table 4.1 Characteristics of Radionuclide Sources Used for Calibration and Static Measurements

Radionuclide	Active Area (cm^2)	Activity (Emission Rate) (cpm)	Source Backing Material[a]	Surface Coating
C-14	13	12,860	S.S.	0.9 mg/cm^2 aluminized Mylar
C-14	13	959,000	S.S.	0.9 mg/cm^2 aluminized Mylar
Ni-63	15	16,600	Ni	NA
SrY-90	15	36,800	S.S./Kapton/Al	NA
SrY-90	13	8,080	Ni	NA
Tc-99	4.9	940	S.S.	NA
Tc-99	4.9	83,400	S.S.	NA
Tc-99	126	26,300	S.S./Al	NA
Tc-99	150	14,400	S.S.	NA
Tl-204	15	6,920	S.S.	NA
Th-230	150	25,100	S.S.	NA
Th-230	126	28,200	S.S./Al	NA
Th-230	5.1	52,700	Ni	NA
Pu-239	5.1	46,300	Ni	NA

[a]S.S. is stainless steel.

Table 4.2 Average Total Efficiencies for Various Detectors and Radionuclides

Radionuclide (Average β Energy)	Total Efficiency (Counts per Disintegration)[a]				
	Gas Proportional			GM	ZnS
	α Only	β Only	α+β		
Beta					
Ni-63 (17.1 keV)	---[b]	---	0.08[c],0.06[d]	0.0025	---
C-14 49.4 (49.4 keV)	---	0.04[e]	0.11[d]	0.05	---
Tc-99 (84.6 keV)	---	0.16[e]	0.22[d]	0.17	---
Tl-204 (244 keV)	---	0.29[e]	0.35[d]	0.26	---
SrY-90 (563 keV)	---	0.36[e]	0.42[d]	0.32	---
Ru-106/Rh-106 (1410 keV)	---	0.55[e]	0.57[c]	0.56	---
Alpha					
Th-230	0.19[d]	---	---	---	0.18
Pu-239	---	---	---	---	0.19

[a]The total efficiencies represent average values compiled from historical instrument calibration data. These values should be considered as the ideal efficiencies obtained under laboratory conditions. Note that calibration sources were typically on stainless steel or nickel backing material.
[b]Data not obtained.
[c]For window density thickness of 0.4 mg/cm^2.
[d]For window density thickness of 0.8 mg/cm^2.
[e]For window density thickness of 3.8 mg/cm^2.

Table 4.3 Minimum Detectable Concentrations for Various Detectors and Radionuclides

Radionuclide (Endpoint β Energy)	Minimum Detectable Concentration (dpm/100 cm^2)[a]	
	Gas Proportional (α+β)	GM
Ni-63 (66 keV)	1,160[b]	70,000
C-14 (156 keV)	630	3,500
Tc-99 (294 keV)	320	1,000
Tl-204 (763 keV)	200	670
SrY-90 (1415 keV)	170	550

[a]MDCs were calculated on the basis of the ambient background count rates presented in Table 5.1 for the gas proportional detector (α+β mode) and the GM detector, and the total efficiencies in Table 4.2. Probe area corrections of 126 and 20 cm^2, respectively, were made for the gas proportional and GM detectors. The following MDC equation was used for 1-minute counts:

$$MDC = \frac{3 + 4.65\sqrt{C_B}}{KT}$$

[b]MDC calculated using total efficiency for window density thickness of 0.8 mg/cm^2 (0.06 count per disintegration (c/dis)).

Table 4.4 Instrument Efficiencies

Radionuclide	Active Area of Source (cm^2)	Instrument Efficiency[a]				
		α + β	β only	GM	α only	ZnS
C-14	13	0.254 ± 0.006	0.081 ± 0.002	0.099 ± 0.002	---[c]	---
Tc-99	126	0.364 ± 0.029	0.191 ± 0.016	0.193 ± 0.021	---	---
T1-204	15	0.450 ± 0.025	0.355 ± 0.021	0.278 ± 0.017	---	---
SrY-90	13	0.537 ± 0.027	0.465 ± 0.024	0.388 ± 0.020	---	---
Th-230	126	---	---	---	0.349 ± 0.015	0.259 ± 0.013

[a]The instrument efficiency was determined with the detector at contact with the source, separated by two sheets of Mylar (0.22 mg/cm^2 per sheet). The instrument efficiency was calculated by dividing the net count rate by the 2π emission rate of the source.

[b]Uncertainties represent the 95% confidence interval, based on propagating the errors in the calibration source emission rate and in counting statistics.

[c]Measurement not performed.

Table 4.5 Source-to-Detector Distance Effects for β Emitters

Distance From Source (cm)	Normalized Net Count Rate [a,b]					
	Ni-63 (Disc)	C-14 (Disc)	Tc-99 (Disc)	Tc-99 (Distributed)	Tl-204 (Disc)	SrY-90 (Disc)
Contact	1	1	1	1	1	1
0.5	0.381 ± 0.064[c]	0.786 ± 0.047	0.864 ± 0.016	0.803 ± 0.015	0.910 ± 0.024	0.9189 ± 0.0065
1	0.196 ± 0.053	0.648 ± 0.048	0.7779 ± 0.0085	0.701 ± 0.023	0.836 ± 0.026	0.8534 ± 0.0088
2	0.038 ± 0.041	0.431 ± 0.034	0.5920 ± 0.0090	0.503 ± 0.014	0.645 ± 0.033	0.6995 ± 0.0063

[a]Normalized net count rate determined by dividing the net count rate at each distance by the net count rate at contact with the source.
[b]Gas proportional detector operated in the α + β mode was used for all measurements.
[c]Uncertainties represent the 95% confidence interval, based on propagating the counting errors in each measurement.

Table 4.6 Source-to-Detector Distance Effects for α Emitters

Distance From Source (cm)	Normalized Net Count Rate [a,b]		
	Pu-239 (Disc)	Th-230 (Disc)	Th-230 (Distributed)
Contact	1	1	1
0.5	0.808 ± 0.013[c]	0.812 ± 0.010	0.761 ± 0.026
1	0.656 ± 0.015	0.606 ± 0.012	0.579 ± 0.021
2	0.1974 ± 0.0046	0.0423 ± 0.0027	0.0990 ± 0.0093

[a]Normalized net count rate determined by dividing the net count rate at each distance by the net count rate at contact with the source.
[b]Gas proportional detectors operated in the α mode were used for all measurements.
[c]Uncertainties represent the 95% confidence interval, based on propagating the counting errors in each measurement.

Table 4.7 Minimum Detectable Concentrations for Various Source-to-Detector Distances for β Emitters

Distance from Source (cm)	Total Efficiency (c/dis) and Minimum Detectable Concentration (dpm/100 cm^2) [a,b]	
	Eff	MDC
Ni-63		
Contact	0.0360 ± 0.0041[c]	2,000 ± 250
0.5	0.0137 ± 0.0019	5,250 ±760
1	0.0071 ± 0.0018	10,200 ± 2,600
2	0.0014 ± 0.0015	52,000 ± 56,000
C-14		
Contact	0.1006 ± 0.0051	715 ± 51
0.5	0.0790 ± 0.0034	910 ± 61
1	0.0652 ± 0.0040	1,103 ± 88
2	0.0434 ± 0.0029	1,660 ± 140
Tc-99 (Disc)		
Contact	0.250 ± 0.010	287 ± 19
0.5	0.2164 ± 0.0090	332 ± 22
1	0.1947 ± 0.0076	369 ± 24
2	0.1482 ± 0.0060	485 ± 32
Tc-99 (Distributed)		
Contact	0.207 ± 0.016	347 ± 32
0.5	0.166 ± 0.013	433 ± 41
1	0.145 ± 0.012	496 ± 49
2	0.1042 ± 0.0086	690 ± 67
Tl-204		
Contact	0.338 ± 0.015	213 ± 14
0.5	0.308 ± 0.013	234 ± 16
1	0.282 ± 0.013	255 ± 18
2	0.218 ± 0.014	330 ± 27
SrY-90		
Contact	0.464 ± 0.016	154.9 ± 9.5
0.5	0.427 ± 0.014	169 ± 10
1	0.396 ± 0.014	181 ± 11
2	0.325 ± 0.011	221 ± 14

[a]Measurements performed with a gas proportional detector operated in the α + β mode with an 0.8-mg/cm^2 window density thickness.

[b]The instrument background was 355 counts and probe area corrections of 126 cm ^{2} were made for the gas proportional detectors. The following MDC equation was used for 1-minute counts:

$$MDC = \frac{3 + 4.65\sqrt{C_B}}{KT}$$

[c]Uncertainties represent the 95% confidence interval, based on propagating the errors in the calibration source activity and in counting statistics.

Table 4.8 Minimum Detectable Concentrations for Various Source-to-Detector Distances for α Emitters

Distance From Source (cm)	Total Efficiency (c/dis) and Minimum Detectable Concentration (dpm/100 cm^2)[a,b]					
	Pu-239 (Disc)		Th-230 (Disc)		Th-230 (Distributed)	
	Eff	MDC	Eff	MDC	Eff	MDC
Contact	0.2549 ± 0.0053[c]	24 ± 14	0.2495 ± 0.0044	24 ± 15	0.2002 ± 0.097	30 ± 18
0.5	0.2061 ± 0.0036	29 ± 18	0.1910 ± 0.0034	32 ± 19	0.1524 ± 0.0067	40 ± 24
1	0.1672 ± 0.0040	36 ± 22	0.1426 ± 0.0034	43 ± 26	0.1160 ± 0.0052	52 ± 32
2	0.0503 ± 0.0012	121 ± 73	0.00994 ± 0.00069	610 ± 370	0.0198 ± 0.0019	310 ± 190

[a]Measurements performed with a gas proportional detector operated in the α mode with a 0.8 mg/cm^2 window thickness.
[b]The instrument background was 1 count and probe area corrections of 126 cm^2 were made for the gas proportional detectors. The following MDC equation was used for 1-minute counts:

$$MDC = \frac{3 + 4.65\sqrt{C_B}}{KT}$$

[c]Uncertainties represent the 95% confidence interval, based on propagating the errors in the calibration source activity and in counting statistics.

Table 4.9 Window Density Thickness Effects for β Emitters

Window Density Thickness (mg/cm^2)	Total Efficiency (c/dis)[a]					
	Ni-63 (Disc)	C-14 (Disc)	Tc-99 (Disc)	Tc-99 (Distributed)	Tl-204 (Disc)	SrY-90 (Disc)
0.3	0.0695 ± 0.0041[b]	0.1273 ± 0.0032	0.288 ± 0.011	0.227 ± 0.018	0.354 ± 0.018	0.477 ± 0.017
0.4	0.0699 ± 0.0032	0.1302 ± 0.0039	0.291 ± 0.011	0.224 ± 0.018	0.359 ± 0.015	0.482 ± 0.019
0.8	0.0409 ± 0.0020	0.1096 ± 0.0032	0.266 ± 0.011	0.209 ± 0.017	0.342 ± 0.015	0.474 ± 0.017
1.3	---[c]	---	0.247 ± 0.010	0.196 ± 0.016	---	---
1.8	---	---	0.2268 ± 0.0092	0.183 ± 0.015	---	---
2.3	---	---	0.2117 ± 0.0090	0.170 ± 0.013	---	---
2.8	---	---	0.1980 ± 0.0085	0.157 ± 0.012	---	---
3.3	---	---	0.1848 ± 0.0074	0.149 ± 0.012	---	---
3.8	0.0005 ± 0.0011	0.0383 ± 0.0018	0.1638 ± 0.0064	0.129 ± 0.010	0.275 ± 0.012	0.429 ± 0.015

[a]Gas proportional detectors operated in the α + β mode were used for all measurements.
[b]Uncertainties represent the 95% confidence interval, based on propagating the errors in the calibration source activity and in counting statistics.
[c]Measurement not performed.

NUREG-1507 4-14 DECEMBER 1997

Table 4.10 Minimum Detectable Concentrations for Various Window Density Thicknesses

Window Density Thickness (mg/cm^2)	Minimum Detectable Concentration ($dpm/100\ cm^2$)[a,b]					
	Ni-63 (Disc)	C-14 (Disc)	Tc-99 (Disc)	Tc-99 (Distributed)	Tl-204 (Disc)	SrY-90 (Disc)
0.3	1,014 ± 80[c]	554 ± 32	245 ± 16	311 ± 30	199 ± 14	147.9 ± 9.4
0.4	1,016 ± 71	546 ± 33	244 ± 16	317 ± 30	198 ± 13	147.3 ± 9.6
0.8	1,760 ± 120	656 ± 39	270 ± 18	344 ± 32	210 ± 14	151.8 ± 9.6
1.3	---[d]	---	291 ± 19	367 ± 34	---	---
1.8	---	---	317 ± 21	392 ± 38	---	---
2.3	---	---	340 ± 23	423 ± 40	---	---
2.8	---	---	363 ± 24	457 ± 43	---	---
3.3	---	---	389 ± 25	482 ± 46	---	---
3.8	130,000 ± 290,000	1,860 ± 130	435 ± 28	555 ± 52	259 ± 18	166 ± 10

[a]Gas proportional detectors operated in the α + ß mode were used for all measurements.

[b]Background levels were determined for each window density thickness and efficiencies were used from Table 4.9. Probe area corrections of 126 cm^2 were made for the gas proportional detectors. The following MDC equation was used for 1-minute counts:

$$MDC = \frac{3 + 4.65\sqrt{C_B}}{KT}$$

[c]Uncertainties represent the 95% confidence interval, based on propagating the errors in the calibration source activity and in counting statistics.

[d]Measurement not performed.

Table 4.11 Source Geometry Effects on Instrument Efficiency

Source Geometry	Instrument Efficiency[a]				
	Tc-99			Th-230	
	α + β	β only	GM	α only	ZnS
Point (Disc) Source[b]	0.445 ± 0.017[c]	0.253 ± 0.010	0.278 ± 0.012	0.4979 ± 0.0089	0.3304 ± 0.0068
Distributed Source[d]	0.382 ± 0.030	0.199 ± 0.016	0.195 ± 0.023	0.397 ± 0.020	0.313 ± 0.016
Ratio of Point-to-Distributed Source	1.16	1.27	1.42	1.25	1.06

[a]The instrument efficiency was determined by dividing the net count rate by the 2 π emission rate of the source.
[b]The point (disc) source area for both Tc-99 and Th-230 was 5 cm^2.
[c]Uncertainties represent the 95% confidence interval, based on propagating the errors in the calibration source emission rate and in counting statistics.
[d]The distributed source area for both Tc-99 and Th-230 was 126 cm^2.

Table 4.12 Ambient Background Effects

Background[a] (cpm)	Gross Counts (cpm)	Measured Activity[b] (dpm)	MDC [c] (dpm)
53.0 ± 9.2[d]	295 ± 32	1,420 ± 190	220
117 ± 22	375 ± 26	1,520 ± 200	310
145 ± 20	413 ± 56	1,580 ± 350	350
192 ± 26	399 ± 38	1,220 ± 270	400
223 ± 26	458 ± 35	1,380 ± 280	430
291 ± 44	538 ± 54	1,450 ± 410	480
445 ± 46	725 ± 66	1,650 ± 480	590
594 ± 42	815 ± 38	1,300 ± 330	680
1,021 ± 38	1,223 ± 55	1,190 ± 390	890
1,490 ± 100	1,642 ± 91	880 ± 800	1,070

[a]Measurements performed with an Eberline HP-260 GM detector.
[b]Measured activity was calculated by subtracting the background from the gross counts and dividing by a total efficiency of 0.17 counts per disintegration. Gross counts were determined by the average of five 1-minute measurements of a Tc-99 source.
[c]The following MDC equation was used for 1-minute counts and an assumed efficiency of 0.17 counts per disintegration:

$$MDC = \frac{3 + 4.65\sqrt{C_B}}{KT}$$

[d]Uncertainties represent the 95% confidence interval, based on propagating the counting errors in each measurement.

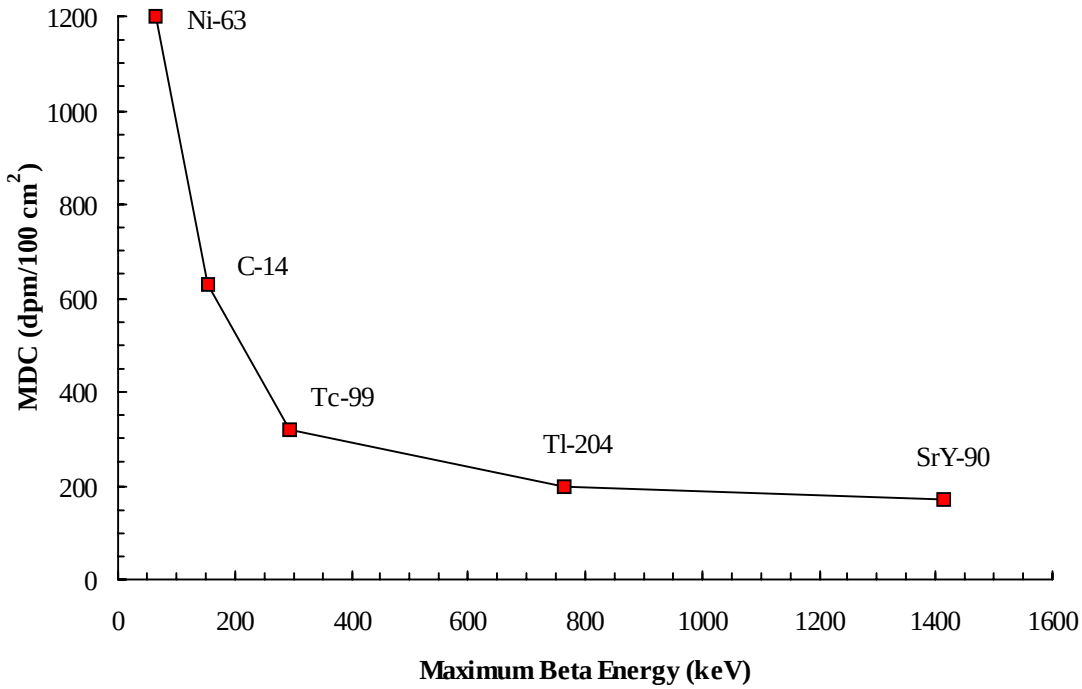

Figure 4.1: MDCs for Gas Proportional Detector ($\alpha+\beta$ Mode) for Various Radionuclides

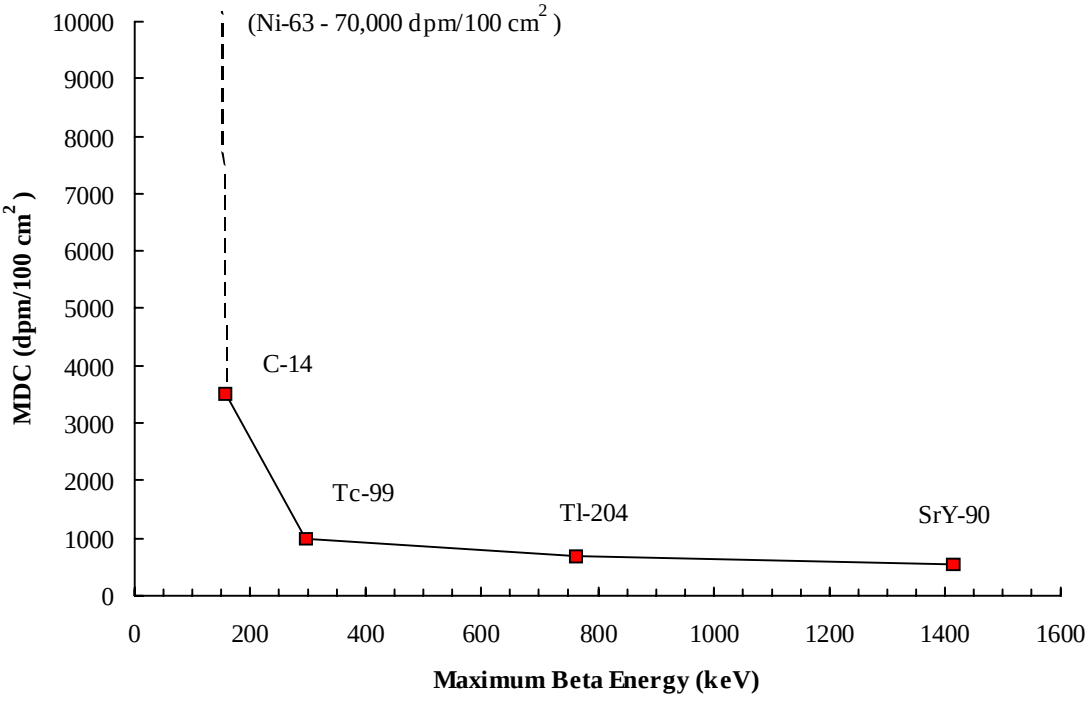

Figure 4.2: MDCs for GM Detector for Various Radionuclides

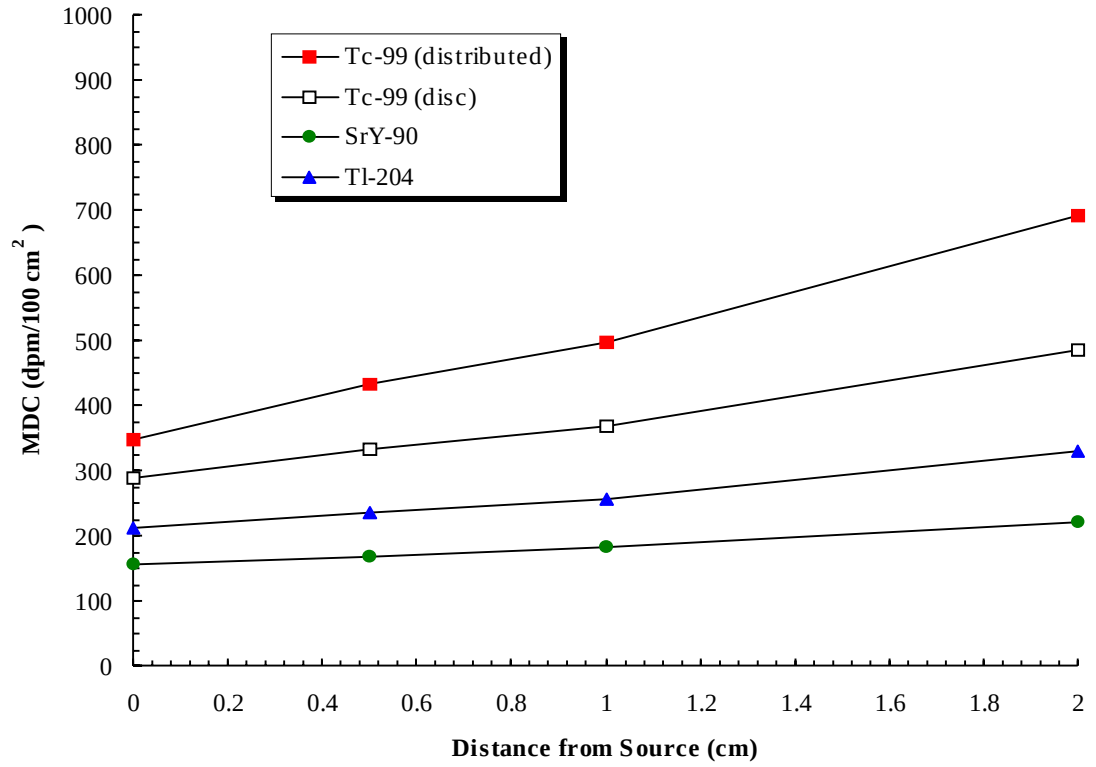

Figure 4.3: Source-to-Detector Distance Effects on MDC for Higher Energy β Emitters

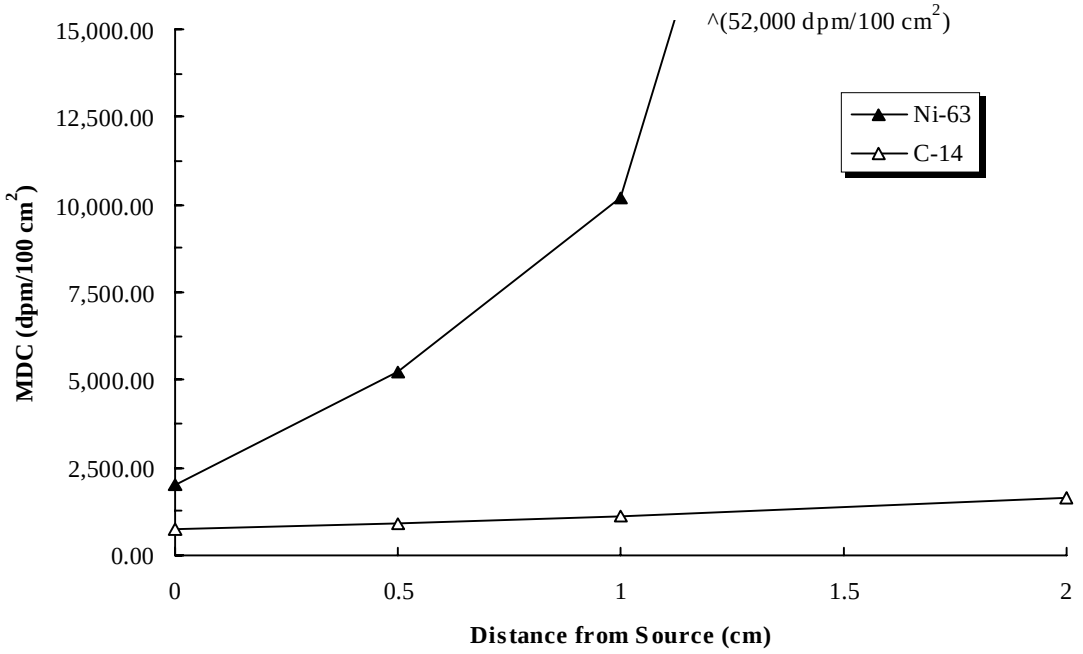

Figure 4.4: Source-to-Dectector Distance Effects on MDC for Lower Energy β Emitters

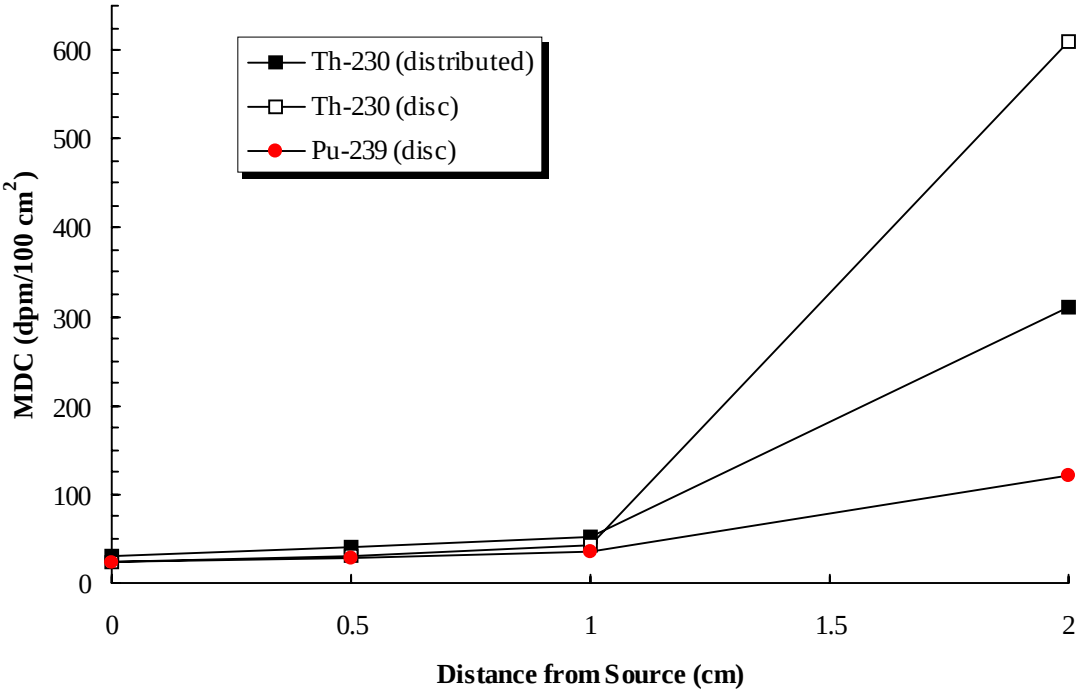

Figure 4.5: Source-to-Detector Effects on MDC for α Emitters

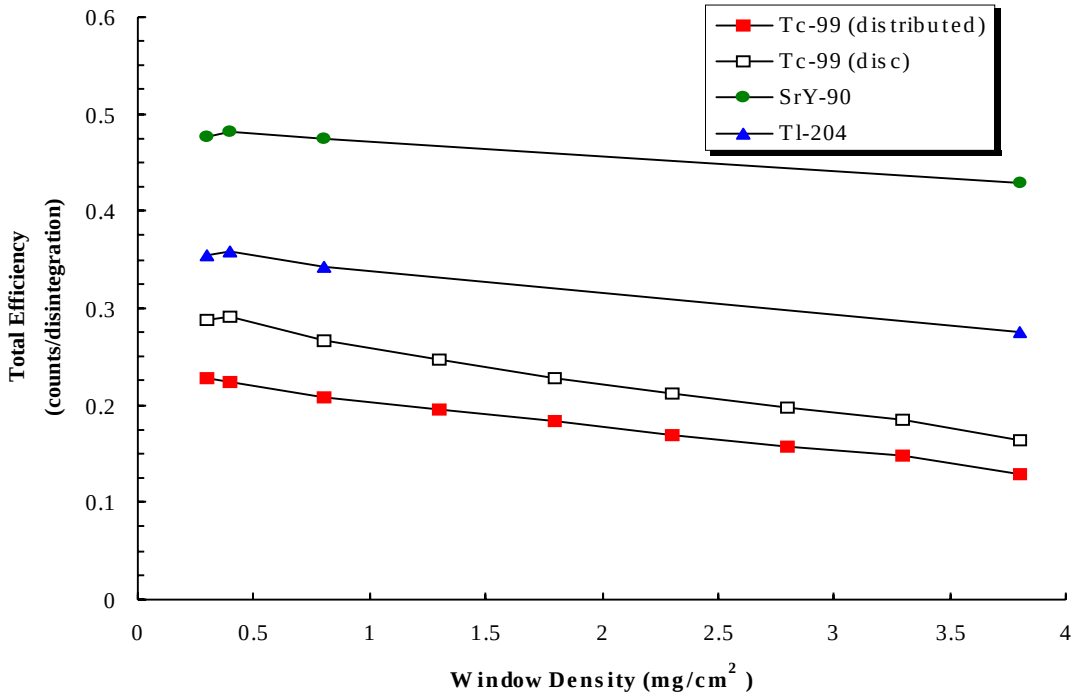

Figure 4.6: Effects of Window Density Thickness on Total Efficiency for Higher Energy β Emitters

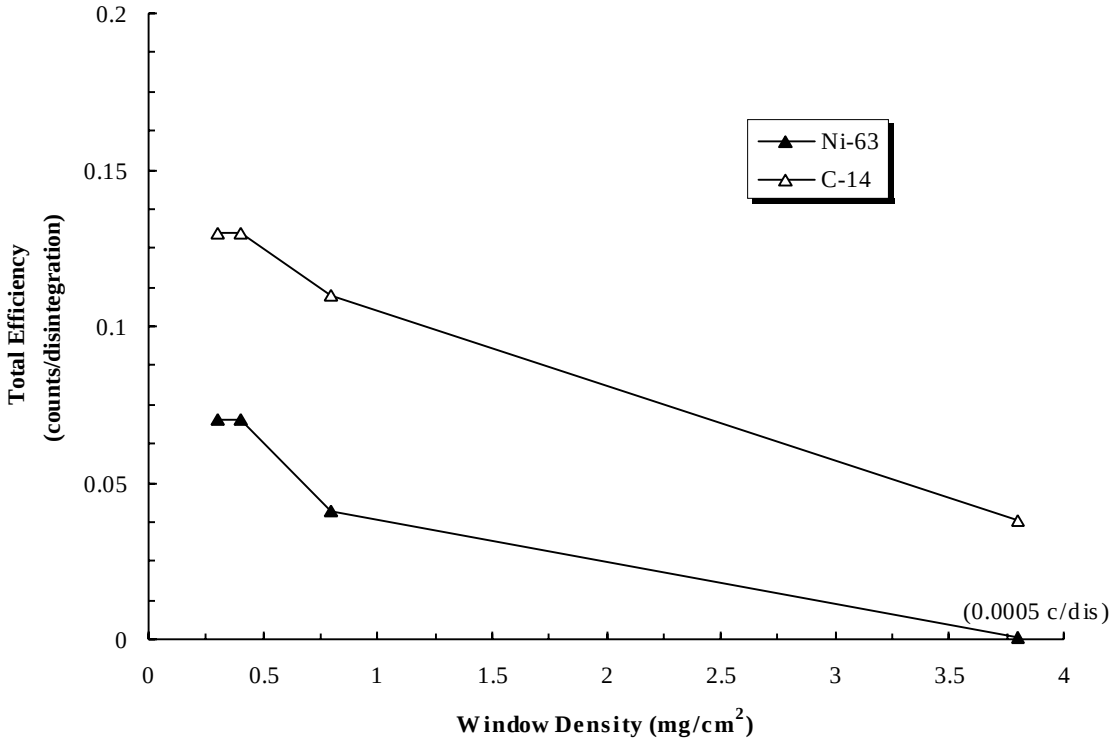

Figure 4.7: Effects of Window Density Thickness on Total Efficiency for Lower Energy β Emitters

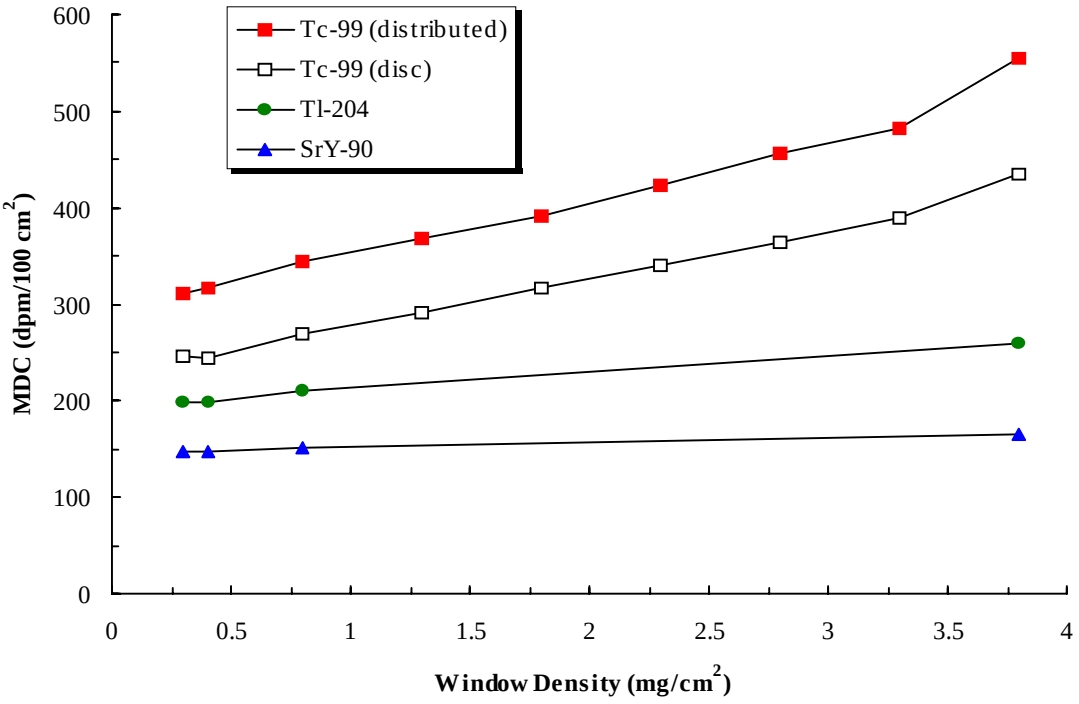

Figure 4.8: Effects of Window Density Thickness on MDC for Higher Energy β Emitters

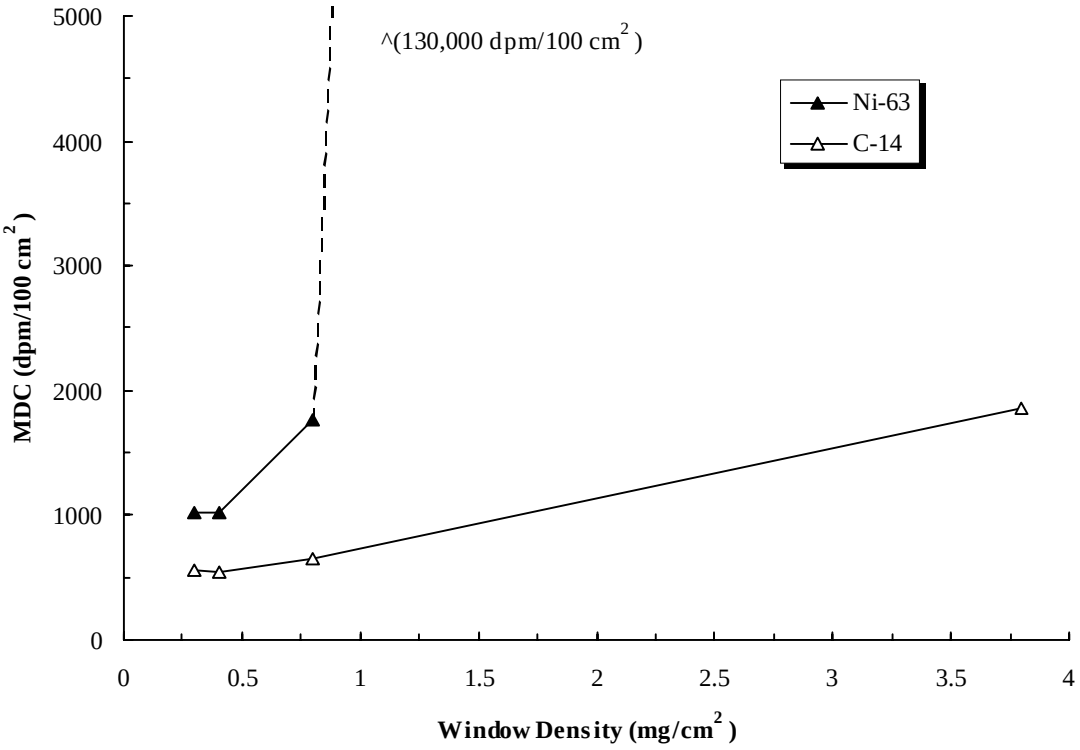

Figure 4.9: Effects of Window Density Thickness on MDC for Lower Energy β Emitters

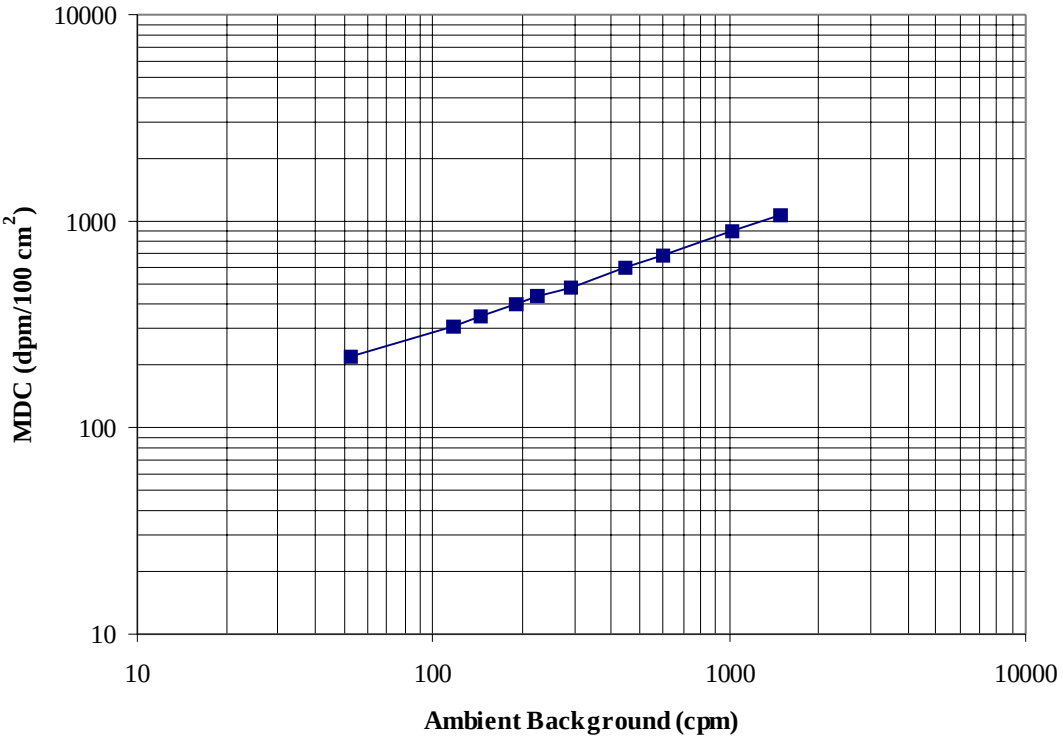

Figure 4.10: Effects of Ambient Background on MDC Calculation